Some aspects of the structure of pp ($\bar{p}p$) scattering at high energy

L. Angelini
Sezione di Bari, Istituto Nazionale di Fisica Nucleare (INFN)
and Dipartimento di Fisica, Università Degli Studi di Bari, Via G. Amendola 173, I-70126 Bari, Italy

L. Nitti
Sezione di Bari, Istituto Nazionale di Fisica Nucleare (INFN), via G. Amendola 173, I-70126 Bari, Italy

M. Pellicoro
Sezione di Bari, Istituto Nazionale di Fisica Nucleare (INFN)
and Dipartimento di Fisica, Università Degli Studi di Bari, Via G. Amendola 173, I-70126 Bari, Italy

G. Preparata
Sezione di Milano, Istituto Nazionale di Fisica Nucleare (INFN)
and Dipartimento di Fisica, Università Degli Studi di Milano, via Celoria 16, I-20133 Milano, Italy
(Received 28 June 1989)

The structure of the high-energy inelastic cross section of pp ($\bar{p}p$) scattering are extensively discussed in terms of the basic quantum-geometrodynamics/anisotropic-chromodynamics mechanism. Predictions on the general structure of final states (charged-particle multiplicities and pseudorapidity distributions) are compared with experimental data at CERN ISR and CERN Collider energies, showing excellent agreement.

I. INTRODUCTION

High-energy hadron-hadron scattering processes have for a long time played a central role in our quest of an understanding of the deep dynamical structure of strong interactions. In recent years, however, one has witnessed a shift of experimental interests toward those processes where one could possibly test theoretical calculations based upon perturbative QCD (PQCD), which is believed to be relevant at short light-cone distances (through the asymptotic-freedom hypothesis). As light-cone-dominated processes make up for only a minute fraction of the events that occur when two high-energy hadrons collide, it turns out that a great deal of the physics which has been uncovered at CERN ISR and $\bar{p}p$ Collider energies has been put aside as too complicated to be described in terms of theoretical concepts that are simple and fundamental enough. This paper, which is the first of a series of theoretical investigations on the structure of pp ($\bar{p}p$) scattering at high energy, wants to address the different aspects of high-energy hadrodynamics within the theoretical framework of a phenomenological model, the quantum-geometrodynamics/anisotropic-chromodynamics (QGD/ACD) fire-string model, with the aim of finding out if and how the simple dynamical description of the model shows up in the experimental data.

As a matter of fact our research program has two main objectives, on one hand to test the basic phenomenological ideas of QGD/ACD and check whether a simple workable picture exists for all aspects of high-energy scattering, and on the other to derive from either success of failure some important suggestions for understanding confinement in QCD, the unchallenged theoretical basis of hadronic behavior.[1]

Before outlining our QCD/ACD program for high-energy hadron-hadron scattering we would like to recall that this theoretical approach has already been applied to high-energy e^+e^--annihilation[2] and to the calculation of deep-inelastic structure functions[3] with remarkably good results, including the prediction of the effect on polarized deep-inelastic μ-p scattering recently observed by the European Muon Collaboration. In addition, several experimental findings have been successfully described and quantitatively analyzed through the QGD/ACD scheme, concerning the pp and $\bar{p}p$ collisions at ISR energies,[4,5] the NA5 effect,[6] and high-p_T physics in pp and $\bar{p}p$ scattering.[7]

The small number of inputs needed to describe most aspects of high-energy physics shows the power of the present approach which, as noted, is based on very simple ideas.

We do not think it necessary to repeat here the key ideas together with their motivations, for this has been done several times (see, for instance, Refs. 2, 8, and 9) in easily accessible journals and books. However, we would like to emphasize that an important difference between QGD/ACD and PQCD, is that the former can be applied also to large-distance physics. Thus, working out the consequences of this approach in high-energy pp ($\bar{p}p$) collisions, as we shall do in this paper, will serve the twofold purpose of further testing the approach and, in case of success, of strengthening the conclusions recently reached about the possible dynamical realization of QCD (Ref. 1). We shall get back on this most relevant point at the end.

The plan of the paper is the following. In Sec. II we

shall analyze and discuss the basic QGD/ACD mechanism of inelastic scattering. Section III will exploit some ideas based on Regge behavior to describe the important mechanisms of high-energy diffraction, while the effects of rescattering of the leading particles shall be analyzed in Sec. IV. In Sec. V the evaluation of the input parameters of the present analysis is discussed in detail. Section VI contains a discussion of the complete inelastic cross section and of the general structure of final states and the comparison of our theoretical predictions with the experimental data. In the final Sec. VII we report our conclusions together with an outline of the future prospects and developments of this work.

II. THE "INELASTIC" SCATTERING MECHANISM

According to QGD/ACD a hadron is a multiquark system ($q\bar{q}$, mesons; qqq, baryons) confined in space regions whose extent is proportional to their mass. Thus, if over a "long" period of time we look at, say, a high-energy proton, we would see the structure depicted in Fig. 1(a). However, if we were take a "snapshot" of the same proton, we would rather see the structure in Fig. 1(b), where both the qqq and $q\bar{q}$ systems are virtual. This is a direct consequence of the Heisenberg principle and of quark-pair creation in the color field of the quarks. Let us now suppose that another hadron, for instance, a proton, impinges on the initial proton, they will scatter only if the color interaction can lead from the initial hadrons to a final state belonging to the allowed (confined) hadronic spectrum.

This implies a well-known feature of hadronic interactions, i.e., their finite range, for color fields do not extend outside the hadrons they permanently bind. In addition it is clear that the individual hadron cross section is definitely larger in configuration (b) than in configuration (a) of Fig 1, this circumstance together with the strong alignment property of the three quarks making up a QGD baryon, imply in turn that the basic "inelastic" scattering diagram is the one described in Fig. 2, whose meaning should be clear. The two incoming protons p_1 and p_2 in the disassociated state

$$p_i(p)\rightarrow B_i(p')+q(k)+\bar{q}(p-p'-k), \quad i=1,2 \qquad (2.1)$$

scatter by giving rise to a final state which is composed of two low-mass excited baryons, B_1 and B_2, and two highly excited mesonic systems, or fire strings, FS_1 and FS_2. The

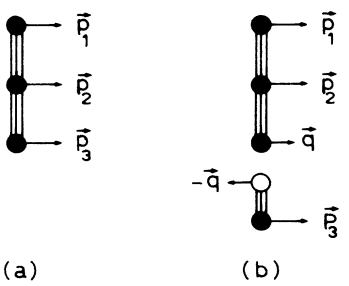

FIG. 1. The proton dissociation in QGD/ACD.

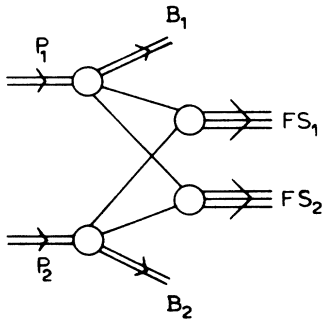

FIG. 2. The basic 2FS mechanism.

mentioned alignment property of QGD/ACD baryons makes it very unlikely that baryonic fire strings are excited in the scattering process. Thus high-energy baryon-baryon scattering, according to QGD/ACD, receives an important contribution from the inelastic process

$$p_1+p_2\rightarrow B_1+B_2+FS_1+FS_2 \qquad (2.2)$$

which leads to a well-defined final state comprising two highly excited mesonic systems (FS_1,FS_2) and two low-mass baryonic resonances (B_1,B_2). We shall refer to the process in Eq. (2.2) as the 2FS mechanism.

The successive decay of both the FS's and the baryonic resonances will produce a host of stable hadrons according to a well-defined pattern, whose structure is precisely predicted in QGD/ACD (Ref. 2). In particular the decay of B_1 and B_2 will produce two high-momentum stable baryons, the well-known "leading" baryons.

In order to proceed from the previous qualitative to a quantitative analysis, our theoretical approach goes through the following steps.

A. The dissociation amplitude

The dissociation process in Eq. (2.1) is calculated under the reasonable assumption that final baryon B is a member of the **56** SU(6) representation, i.e., is a member of the low-lying $\frac{1}{2}^+$ octet and $\frac{3}{2}^+$ decuplet. The neglect of higher mass resonances ($M>1.5$ GeV) is, however, expected to slightly affect only the calculated "leading" particle spectrum (see Sec. VI). With this restriction the dissociation amplitude $A_B(p,p',k)$ can be readily computed from a straightforward overlap integral between the initial and the final QGD baryonic wave functions.[10] The calculation, reported in Appendix A, shows that at high energy the dissociation amplitude scales in the manner of Feynman and exhibits transverse-momentum cutoffs for B and the quark-antiquark pair. Figure 3 shows the Feynman x dependence of the square of the amplitude for the final proton, quark, and antiquark, while in Fig. 4 the relevant transverse-momentum distributions are reported. Note the rather hard x spectrum of the proton ($\langle x_p\rangle=0.6$), as compared with the soft quark spectrum ($\langle x_q\rangle=0.3$) and the still softer antiquark spectrum ($\langle x_q\rangle=0.1$). For the transverse-momentum distributions, the leading-baryon spectrum shows a very steep

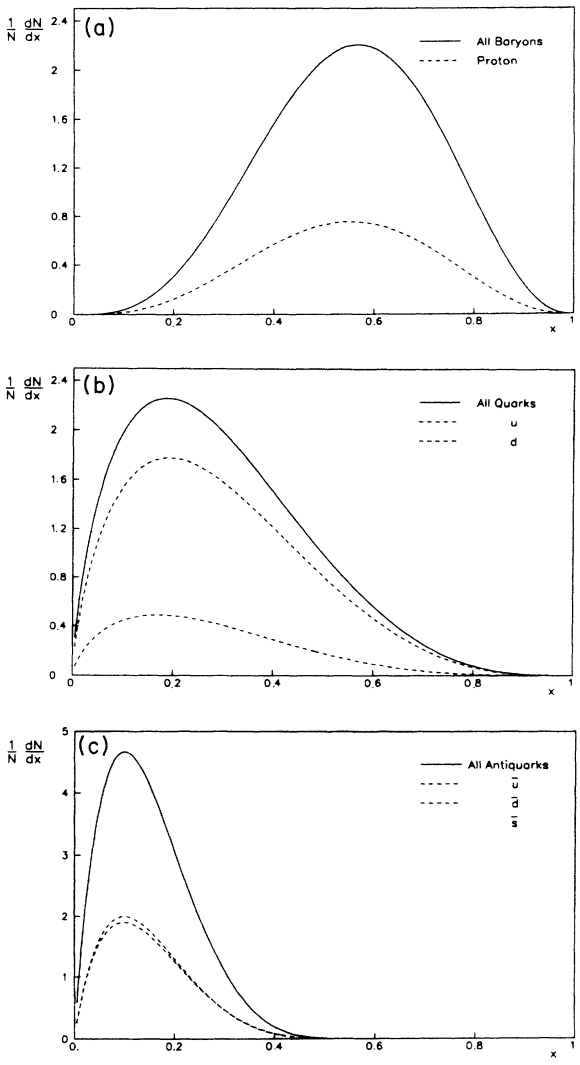

FIG. 3. The x spectrum of (a) the leading baryon; (b) the quark; and (c) the antiquark in the 2FS mechanism.

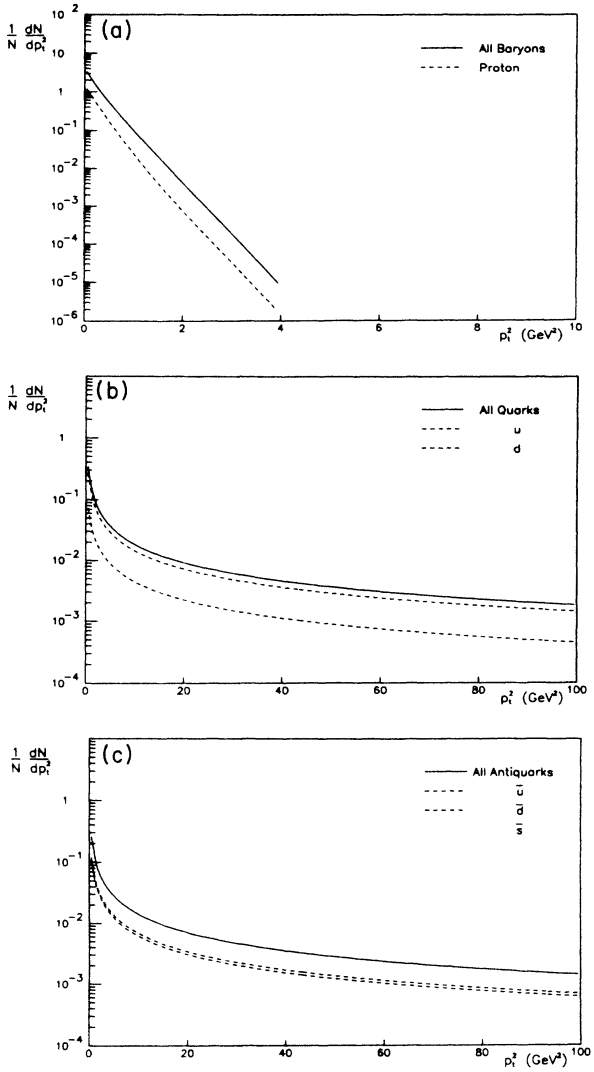

FIG. 4. The p_T dependence of (a) the leading baryon; (b) the quark; and (c) the antiquark of the 2FD mechanism.

behavior, while the quark and antiquark spectra reveal a long tail due to the hard scattering of a quark or an antiquark of the upper vertex with a quark or an antiquark of the lower vertex, before the two pairs arrange themselves in the fire strings FS_1 and FS_2 of Eq. (2.2) (Ref. 7).

B. The "inelastic" (2FS) cross section

By squaring the diagram in Fig. 2 and summing over all final states we obtain the contribution σ_{2FS} to the total inelastic cross section of the 2FS mechanism (the relative diagram is reported in Fig. 5). Once the structure of the dissociation amplitudes is known, there is no problem to evaluate the energy dependence of $\sigma_{2FS}(s)$. Indeed the diagram for $\sigma_{2FS}(s)$ involves the integration over the four-momenta k_1, k_2 of the baryonic resonances and the four-momenta q_1, q_2 of the initial quarks and one of the four-momenta q_1' of the final quarks. The integration over q_1' can be readily carried out by the fact that quarks are close to their "mass shell" and exploiting the fact that the FS amplitudes are peaked in the quark momentum-transfer, i.e.,

$$G(q_1,q_1') \to \sum_i \beta_i s^{\alpha_i(0)} e^{b_i(q_1-q_1')^2} , \tag{2.3}$$

where the sum runs over the "leading" Reggeons, namely, P with $\alpha_P(0)=1$, and R with $\alpha_R(0)=\frac{1}{2}$. Thus, proceeding along the lines of Ref. 11, we arrive at the expression

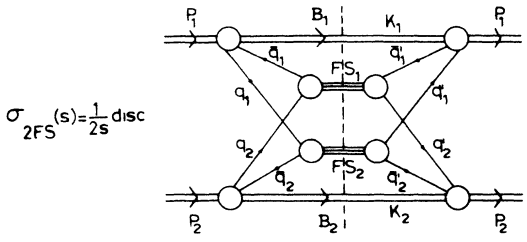

FIG. 5. The diagram describing the cross section of the 2FS mechanism.

$$s\sigma_{2FS}(s)=\sum_{ij}\beta_i\beta_j\int\frac{d^3k_1}{2E_1(2\pi)^3}\int\frac{d^3k_2}{2E_2(2\pi)^3}\int\frac{d^4q_1}{(2\pi)^4}\int\frac{d^4q_2}{(2\pi)^4}|A(p_1,k_1,q_1)|^2|A(p_2,k_2,q_2)|^2\frac{s_1^{\alpha_i(0)}s_2^{\alpha_j(0)}}{16\pi R^2(b_is_1+b_js_2)}\ , \tag{2.4}$$

where $R^2=2$ GeV^{-2} is a dimensional parameter, and $s_1=(q_1+\bar{q}_2)^2$ and $s_2=(\bar{q}_1+q_2)^2$ are the masses squared of the two fire strings. In view of the mentioned scaling properties of the dissociation amplitudes, it is easy to see that the asymptotic behavior of $\sigma_{2FS}(s)$ is given by

$$\sigma_{2FS}\to a_1+\frac{a_2}{\sqrt{s}},\quad s\to\infty\ . \tag{2.5}$$

Several remarks concerning Eqs. (2.4) and (2.5) are now called for. The Regge-like behavior of the high-energy limit of σ_{2FS} is not an input in QGD/ACD but is a consequence of its scaling, finite range, and spectrum properties. Indeed, the constant term originates from finite range and scaling, while the $s^{-1/2}$ term is a consequence of the existence of Regge trajectories with the right intercept and slope. As for Eq. (2.4), it gives an explicit expression for the composition of the final state, namely, the FS distributions and the baryon spectra. We shall return on this point at the end. Finally, the value of the constants a_1 and a_2 in Eq. (2.5) cannot be computed from the model, due to our lack of knowledge of the normalizations of the dissociation amplitude, the "Regge" residues β_i''s and the slopes b_i''s. However we should point out that in order to describe $\sigma_{2FS}(s)$ for any baryon (antibaryon)-baryon scattering we need only two parameters.

III. THE DIFFRACTION MECHANISMS

In the preceding section we have discussed the simplest contribution $\sigma_{2FS}(s)$ to the inelastic hadron-hadron cross section at high energy. The problem we wish to address now is to determine how such an elementary mechanism influences high-energy diffraction which, as we know, plays a very important role at very high energies.

A. Single-diffractive mechanism

Let us go back to $\sigma_{2FS}(s)$. According to the optical theorem

$$\sigma_{2FS}(s)=\frac{1}{s}\mathrm{Im}\,A_{2FS}(p_1p_2\to p_1p_2)\ , \tag{3.1}$$

where $A_{2FS}(p_1p_2\to p_1p_2)$ is the forward-scattering amplitude, calculated in the approximation discussed in Sec. II (see Fig. 5). Thus to this mechanism there corresponds a well-defined elastic amplitude $A_{2FS}(p_1p_2\to p_1'p_2')$ that can be thought of as the "shadow" of the inelastic processes described by the 2FS mechanism of the preceding section. We may now ask what happens in the QGD/ACD calculation when we substitute a final proton, say p_1', with a more complicated state. It is clear that in this way one is computing a contribution to the "single-diffractive" (SD) cross section. Let us go back to the diagram in Fig. 5, by representing the sum over the FS's by a wavy "Pomeron" line.[12] We obtain the diagram in Fig. 6(a). Now the dominant high-mass SD amplitude is, according to QGD/ACD, given by exchanging the "primeval Pomerons" between the lower (upper) vertex and a $q\bar{q}$ pair generated in a double dissociation of the proton $p_1(p_2)$ [see Fig. 6(b)]. Note that the curly line denotes the "QGD gluon" discussed in Ref. 2. Thus the inelastic state produced by the SD mechanism comprises a baryonic low-mass resonance and two FS's.

In order to appreciate why the diagram in Fig. 6(b) dominates high-mass single diffraction we need only recall that one of the basic postulates of QGD/ACD is that, in a given class of processes, the dominant diagrams are those that involve the smallest number of quark lines.

The reason why we need consider an extra $q\bar{q}$ pair in the process of proton dissociation, is that it has been shown long ago[11] that at high mass two-FS production dominates over single-FS production. The diagram in Fig. 6(b) can be further simplified, by using the factorization properties that it enjoys a high energy, to the one reported in Fig. 7(a), where the double wavy line describes the "effective" Reggeon (P and R) resulting from the 2FS mechanism [see Eq. (2.5)]. When we square the amplitude in Fig. 7(a) we obtain the diagram reported in Fig. 7(b), which can be immediately recognized to yield the standard Regge form for single diffraction,[13] i.e.,

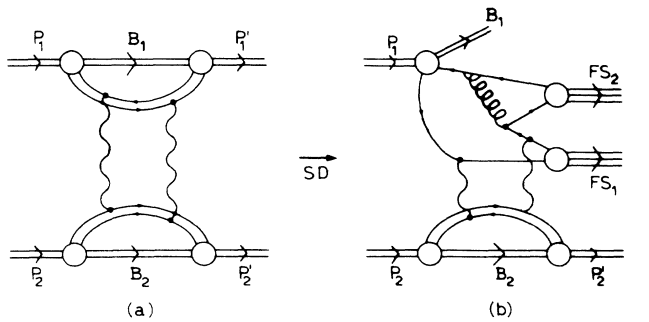

FIG. 6. (a) The Regge representation and (b) the QGD/ACD implementation of the single-diffractive mechanism.

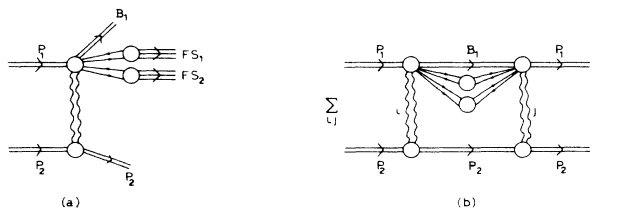

FIG. 7. The single-diffractive inelastic (a) amplitude and (b) cross section in the triple Regge approximation.

$$\frac{s}{\pi}\frac{d\sigma_{\rm SD}}{dt\,dM^2}=\frac{1}{16\pi^3}\sum_{ijk}\beta_i(t)\beta_j(t)\left[\frac{s}{M^2}\right]^{\alpha_i(t)+\alpha_j(t)-\alpha_k(0)}\beta_k(0)g_{ijk}(t)\left[\frac{s}{m^2}\right]^{\alpha_k(0)-1}, \tag{3.2}$$

where $M^2\simeq s(1-x)$ is the invariant mass of the diffractively produced system of two FS's plus a baryon resonance. A precise calculation of the QGD/ACD diagram in Fig. 7(b), even though possible, will require a considerable computing effort. Thus, for the time being, we shall content ourselves with the compatibility of Eq. (3.2) with QGD/ACD, and shall extract the functions $\beta_i(t)$ and $g_{ijk}(t)$ from experiments. In this paper we shall consider the two terms of Eq. (3.2) corresponding to $(i=j=k=P)$ and $(i=j=R,\ k=P)$, thus obtaining

$$\frac{s}{\pi}\frac{d\sigma_{\rm SD}}{dt\,dM^2}=G_{PPP}\left[\frac{s}{M^2}\right]^{2\alpha_P(t)-\alpha_P(0)}+G_{RRP}\left[\frac{s}{M^2}\right]^{2\alpha_R(t)-\alpha_P(0)}. \tag{3.3}$$

In Eq. (3.2) the dominant term at high energy is obtained by choosing $i=j=k=P$, i.e.,

$$\frac{d\sigma_{\rm SD}}{dt\,d\xi}=\frac{\beta_P(0)\beta_P^2(t)g_{3P}(t)}{16\pi^2}e^{-2\alpha_P'(0)t\xi} \tag{3.4}$$

where $\xi=\ln(M^2/s)$. Using the parametrizations of $\beta_P(t)$ and $g_{3P}(t)$, for t not too large, given in Appendix B, Eqs. (B7a) and (B7b), we obtain, after the t integration,

$$\sigma_{\rm SD}(s)=\frac{\beta_P^3(0)g_{3P}(0)}{16\pi^2}\int_{\xi_{\min}}^{\xi_{\max}}\frac{d\xi}{2(b_0+b_1)-2\alpha_P'(0)\xi}=\frac{\beta_P^3(0)g_{3P}(0)}{32\pi^2\alpha_P'(0)}\ln\frac{b_0+b_1-\alpha_P'(0)\xi_{\min}}{b_0+b_1-\alpha_P'(0)\xi_{\max}}, \tag{3.5}$$

where

$$\xi_{\min}=\ln(M_{\min}^2/s),\qquad \xi_{\max}=\ln(M_{\max}^2/s)\simeq\ln(1-x_1), \tag{3.6}$$

with $M_{\min}^2\simeq 1$ GeV^2 and $x_1\simeq 0.9$, are the appropriate limits in the ξ integration. However in our numerical implementation of the present approach, we make use of Eq. (3.2) in the full phase space.

Notice that the SD cross section, unlike $\sigma_{\rm 2FS}(s)$ which is asymptotically constant, increases linearly with $\ln[\ln(s)]$.

B. Double-diffractive mechanism

By now it should be clear how to proceed to describe the phenomenon of double diffraction (DD). We need only substitute in Fig. 7(b) the lower part with the mirror image of the upper part, thus obtaining the diagram in Fig. 8. Again little effort is needed to conclude the QGD/ACD amplitude has the Regge structure (only the P trajectory is considered):

$$\frac{d\sigma_{\rm DD}}{d\xi_1 d\xi_2 dt}=\frac{1}{16\pi^3}\beta_P^2(0)g_{3P}^2(t)e^{2[\alpha_P(t)-1]\xi'}\left[\frac{M_1^2M_2^2}{m^4}\right]^{\alpha_P(0)-1}, \tag{3.7}$$

where M_1 and M_2 are the invariance masses of the two diffractive systems, m is the proton mass, and

$$\xi'=\ln\left[\frac{sm^2}{M_1^2M_2^2}\right],\quad \xi_i=\ln\left[\frac{M_i^2}{m^2}\right],\quad i=1,2. \tag{3.8}$$

The function $g_{3P}(t)$ is the 3-Pomeron vertex already encountered for single diffraction in Eq. (3.4). As for the SD mechanism, the complete computation of the QGD/ACD diagram would require a massive computational effort; thus we shall, for the time being, content ourselves with fitting the functions $\beta_P(t)$ and $g_{3P}(t)$ from experiments.

Using the parametrization of $g_{3P}(t)$, for t not too large, given in Appendix B, Eq. (B7b), one obtains

$$\sigma_{\rm DD}(s)=\frac{\beta_P^2(0)g_{3P}^2(0)}{16\pi^3}\int_{\xi_0}^{\xi-\Delta-\xi_0}d\xi_1\int_{\xi_0}^{\xi-\Delta-\xi_1}\frac{d\xi_2}{4b_1+2\alpha_P'(0)(\xi-\xi_1-\xi_2)}=\frac{\beta_P^2(0)g_{3P}^2(0)}{32\pi^3[\alpha_P'(0)]^2}\left[[2b_1+(\xi-2\xi_0)\ln\frac{2b_1+\alpha_P'(0)(\xi-2\xi_0)}{2b_1+\alpha_P'(0)\Delta}-\alpha_P'(0)(\xi-\Delta-2\xi_0)\right], \tag{3.9}$$

where $\Delta\simeq 1$ is the minimum rapidity gap between the diffractive clusters and

$$\xi=\ln\left[\frac{s}{m^2}\right],\qquad \xi_0=\ln(M_{\min}^2/m^2)\simeq\ln[(m_p+m_\pi)^2/m_p^2]. \tag{3.10}$$

Notice that, for very high energy,

$$\sigma_{\rm DD}(s)\sim\ln(s)\ln[\ln(s)]. \tag{3.11}$$

We would like to emphasize that once the parameters needed to completely specify $\sigma_{\rm 2FS}(s)$ and $\sigma_{\rm SD}(s)$ are supplied, Eq. (3.9) determines $\sigma_{\rm DD}(s)$, with no extra input.

The contribution of the three basic mechanisms (2FS, SD, DD) to the elastic-scattering amplitude are calculated in Appendix B.

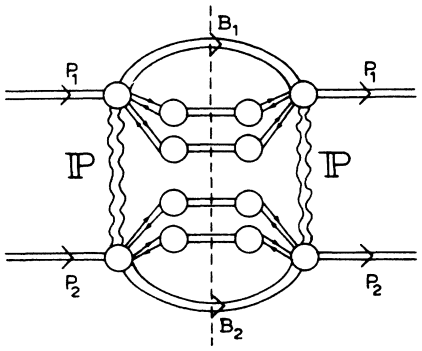

FIG. 8. The diagram representing the double-diffractive inelastic cross section.

IV. THE RESCATTERING MECHANISMS

So far we have considered that class of high-energy processes that have the common feature of being free of any final-state interaction. While according to QGD/ACD these processes are supposed to dominate, there is nevertheless a finite probability that the hadronic structures produced in the final states according to the three mechanisms 2FS, SD, DD (which from now on we shall call first-order mechanisms), described in the preceding sections, do undergo a further interaction. This is the subject of the present section.

In the final states produced by the first-order mechanisms we have two types of structures: leading baryons and fire strings. We shall now demonstrate that the final-state interactions of FS's can be neglected, because they are suppressed by factors proportional to the FS mass. Let us consider a simple 2FS-type scattering between two FS's, whose cross section can be calculated from the diagram in Fig. 9. By describing the Pomeron exchange by the helicity-conserving coupling γ_μ, we immediately see that the Regge residue is proportional to the vector-current matrix element p_μ/M. Thus we easily calculate

$$\sigma_{\text{FS-FS}}(s)\to\frac{\beta_0^2}{s}\frac{p_1p_2}{M_1M_2}\simeq\frac{\beta_0^2}{2M_1M_2}\ , \tag{4.1}$$

where β_0 is a fixed geometrical constant. This means that FS's interact very weakly among themselves and with low mass hadrons, so that we can neglect their final-state interactions.

We note, incidentally, that QGD/ACD through Eq. (4.1) gives a simple and elegant explanation of the puzzling results obtained some time ago by scattering high-energy protons on different nuclei. Contrary to expectations it was found that the final-state multiplicity changes only little by going from the H nucleus to the heaviest nuclei, thus implying that no intranuclear cascade process takes place. According to QGD/ACD the absence of an intranuclear cascade process is simply related to the fact that the nucleus is almost transparent to FS's, and that the FS-decay time into stable hadrons is long (it increases linearly with the FS mass). All this means that the bulk of the multiparticle production, according to QGD/ACD, takes place far away from the interaction region.

Getting back to the problem of final-state interaction, we reach the important conclusion that only the low-mass "leading particles" may reinteract. Let us see how.

All of the first-order scattering mechanisms $i=$(2FS, SD, DD) are of the type

$$p_1+p_2\to B_1+B_2+(\text{FS's}) \tag{4.2}$$

and can be diagrammatically represented as in Fig. 10(a). In Fig. 10(b) we have represented the rescattering diagram, originating from the first-order mechanism i.

In order to compute the rescattering cross section we shall proceed, according to the QCD/ACD strategy, in a perturbative fashion and, due to the notable coherence properties of the FS production, we have the possibility of dealing with diagrams in cascade. We specify the "black box" of Fig. 10(b) as any one of the first-order mechanisms j and make the very reasonable assumption (Pomeron dominance) that the B_1B_2 scattering amplitude for any of the first-order mechanism j is universal and can be parametrized at high energy as

$$A_j(B_1B_2\to B_1'B_2')=s\sigma_j(s)e^{b_jt}\delta_{B_1B_1'}\delta_{B_2B_2'} \tag{4.3}$$

with the slope b_j calculated in Appendix B.

A straightforward calculation then shows that, calling $\sigma_{ij}(s)$ the cross section for the final-state interaction of type j originating from the process of type i, we have

$$\sigma_{ij}^{(2)}(s)=\frac{\sigma_i(s)}{16\pi}\int_0^s f_i(s,s')\frac{\sigma_j(s')}{b_j(s')}ds'\ , \tag{4.4}$$

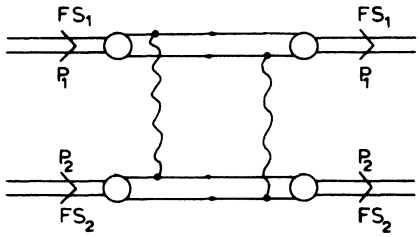

FIG. 9. The diagram representing the FS-FS scattering amplitude.

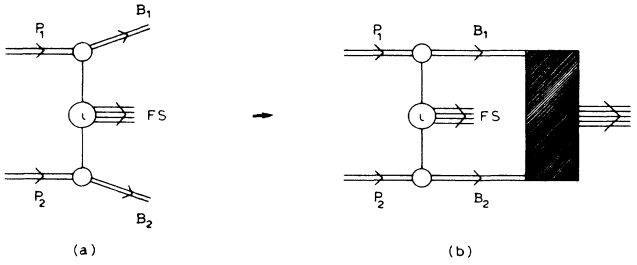

FIG. 10. (a) The first-order scattering mechanism i and (b) the rescattering diagram originating from the first-order mechanism i.

where $f_i(s,s')$ is a known function, normalized to unity, defined by

$$f_i(s,s')=\frac{K_i(s,s')}{\sigma_i(s)} \tag{4.5}$$

(see Appendix B), whose form is calculated from the momentum distributions of the leading baryon.

The simple structure of the rescattering diagrams allow us to describe with no extra effort the nth-order scattering, from the $(n-1)$th-order scattering. Calling $\sigma^{(n)}_{i_1 i_2 \cdots i_n}(s)$ the cross section for the sequence $i_1 i_2 \cdots i_n$ of scattering mechanisms (i_k=2FS, SD, DD), we have the simple generalization of Eq. (4.4):

$$\sigma^{(n)}_{i_1 i_2 \cdots i_n}(s) = \frac{\sigma^{(n-1)}_{i_1 i_2 \cdots i_{n-1}}(s)}{16\pi} \int_0^s f_{i_1 i_2 \cdots i_{n-1}}(s,s') \frac{\sigma_{i_n}(s')}{b_{i_n}(s')} ds' , \tag{4.6}$$

where the function $f_{i_1 i_2 \cdots i_{n-1}}(s,s')$ is defined by

$$f_{i_1 i_2 \cdots i_{n-1}}(s,s')=\int_{s'}^{s} f_{i_1}(s,s_1)ds_1 \int_{s'}^{s_1} f_{i_2}(s_1,s_2)ds_2 \cdots \int_{s'}^{s_{n-3}} f_{i_{n-2}}(s_{n-3},s_{n-2}) f_{i_{n-1}}(s_{n-2},s')ds_{n-2} \tag{4.7}$$

with the normalization condition

$$\int_0^s f_{i_1 i_2 \cdots i_{n-1}}(s,s')ds'=1 \tag{4.8}$$

and enjoys nice scaling properties.

Calling

$$\sigma^{(n)}(s)=\sum_{i_1 \cdots i_n} \sigma_{i_1 \cdots i_n}(s) , \tag{4.9}$$

the inelastic cross section is given by

$$\sigma_{in}(s)=\sum_n \sigma^{(n)}(s) . \tag{4.10}$$

Notice that the inelastic cross section, as calculated in the present section can only be partially compared to the experimental cross section, because the absorption mechanism has not been taken into account, for this interesting problem is beyond the scope of this paper.

V. THE INPUT PARAMETERS

We are now going to compare our theoretical developments with experimental data. As emphasized in the previous sections we need the following inputs.

(i) The Regge trajectories $\alpha_P(t)$ and $\alpha_R(t)$, parametrized in the standard form

$$\alpha_P(t)=1+\alpha'_P(0)t, \quad \alpha'_P(0)=0.2 \text{ GeV}^{-2} , \tag{5.1a}$$

$$\alpha_R(t)=\tfrac{1}{2}+\alpha'_R(0)t, \quad \alpha'_R(0)=0.75 \text{ GeV}^{-2} . \tag{5.1b}$$

(ii) The Regge residue functions parametrized as

$$G(t)=G(0)e^{bt+ct^2+dt^3} . \tag{5.2}$$

The parameters, entering in Eq. (5.2), have been determined by fitting the leading-proton experimental data[12] in the diffractive peak region ($x \simeq 1$), where the SD mechanism largely dominates the invariant cross section $E\,d^3\sigma/dp^3$. For PPP the fit gives the values

$$G(0)=1.49 \text{ mb/GeV}^2 ,$$
$$b=5.81 \text{ GeV}^{-2} , \tag{5.3a}$$
$$c=2.71 \text{ GeV}^{-4}, \quad d=0.53 \text{ GeV}^{-6} ,$$

and for RRP we get

$$G(0)=9.55 \text{ mb/GeV}^2 ,$$
$$b=5.40 \text{ GeV}^{-2} , \tag{5.3b}$$
$$c=5.77 \text{ GeV}^{-4}, \quad d=1.98 \text{ GeV}^{-6} .$$

(iii) The parameters a_1 and a_2 of Eq. (2.5) with the constraint that the $s^{-1/2}$ term must be small compared to a_1 at the energies of the present analysis. Therefore a_1 and a_2 are free parameters.

(iv) The parameters (b_{2FS}, b_0, b_1, b_3), defined in Appendix B, must satisfy the following constraints: (a) leading proton slope [see Eq. (5.2)]

$$b_{PPP}=2(b_0+b_1) ; \tag{5.4}$$

(b) elastic scattering slope [see Eq. (B12)]

$$B_{el}=2\left[b_{2FS}\frac{\sigma_{2FS}}{\sigma^{(1)}}+b_{SD}\frac{\sigma_{SD}}{\sigma^{(1)}}+b_{DD}\frac{\sigma_{DD}}{\sigma^{(1)}}\right] . \tag{5.5}$$

Then, the six effective parameters $a_1, a_2, b_{2FS}, b_0, b_1, b_3$, constrained by the two conditions of Eqs. (5.4) and (5.5) leave us with 4 degrees of freedom that have been fixed by the present analysis, as illustrated in the following section.

The best-fit values are

$$a_1=4.8 \text{ mb} , \tag{5.6a}$$
$$a_2=50 \text{ mb GeV} , \tag{5.6b}$$
$$b_{2FS}=2.2 \text{ GeV}^{-2} , \tag{5.6c}$$
$$b_0=2.20 \text{ GeV}^{-2} , \tag{5.6d}$$
$$b_1=0.70 \text{ GeV}^{-2} , \tag{5.6e}$$
$$b_3=1.85 \text{ GeV}^{-2} . \tag{5.6f}$$

VI. COMPARISON WITH EXPERIMENTS

Once the fire strings get formed with the various mechanisms described in the preceding sections, they decay in a sequential way as explained in detail in Ref. 2. The re-

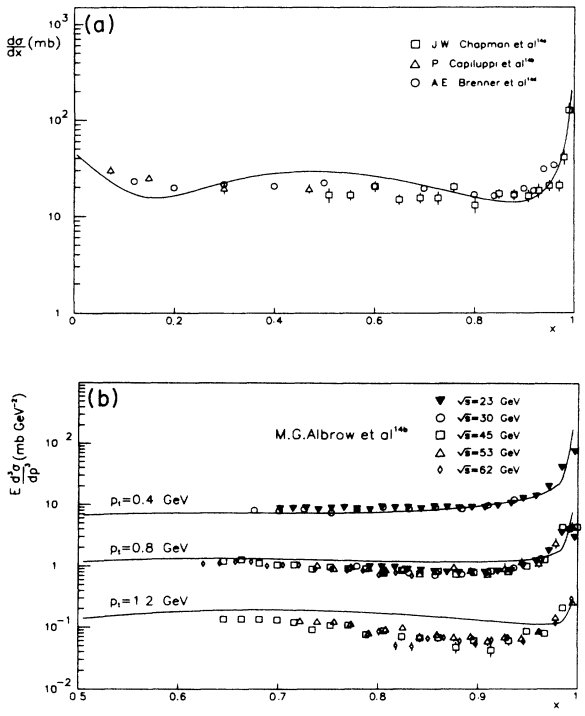

FIG. 11. Comparison between the experimental data (Ref. 14) and our prediction for (a) the differential cross section $d\sigma/dx$ and (b) the invariant distribution $E\,d^3\sigma/dp^3$ as a function of x at $p_T=0.4$, 0.8, 1.2 GeV^2.

sults, exposed in this paper, are obtained by the Monte Carlo method.

The simple parametrizations in Eqs. (5.1) and (5.2) and the parameters' values in Eq. (5.3) can be seen to reproduce rather well the experimental information[14] on the proton Feynman x distribution reported in Fig. 11.

With the values of the parameters $a_1, a_2, b_{2FS}, b_0, b_1, b_3$ given in Eq. (5.6) we compute the energy dependence of the inelastic cross section $\sigma_{in}(s)$, that is compared with experimental data[15] in Fig. 12. As one can see the theoretical cross section is in rather good agreement with the data, especially in view of our complete neglect of absorption effects, which in the Collider region are known

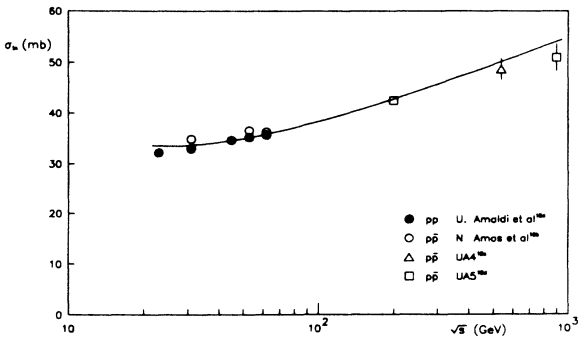

FIG. 12. Our prediction for the pp ($\bar{p}p$) inelastic cross section compared to the experiments (Ref. 15).

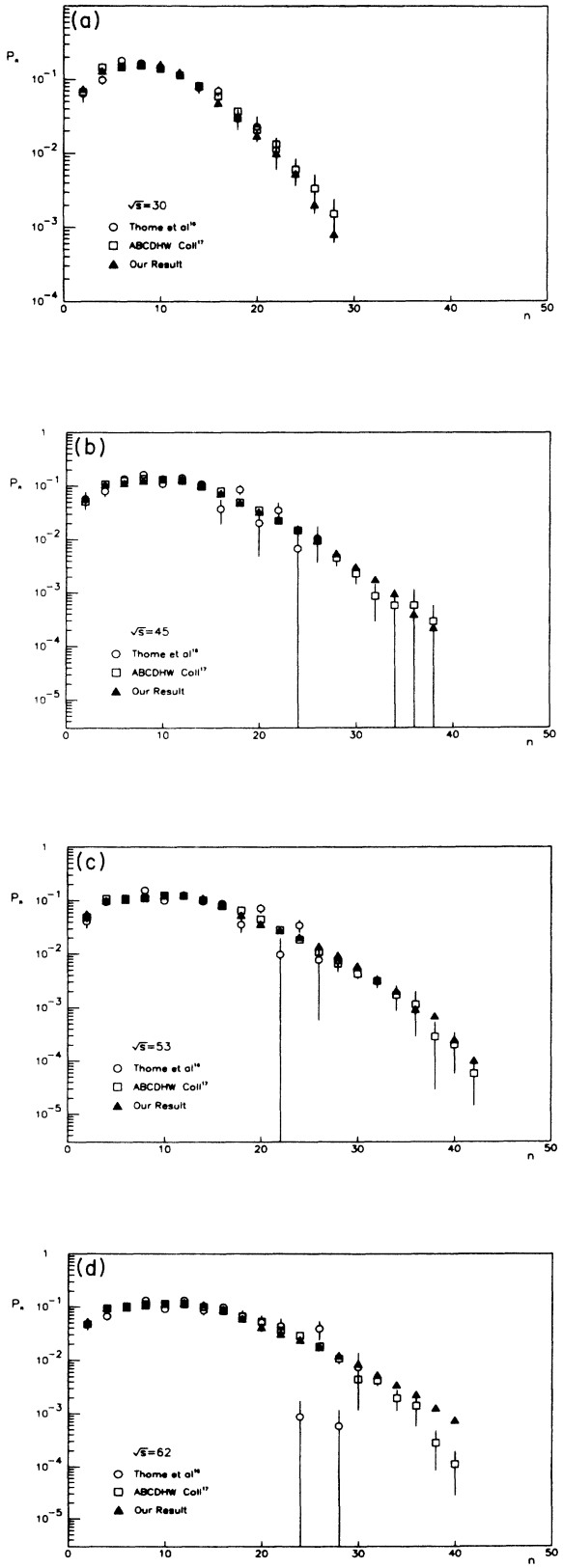

FIG. 13. Comparison between the experimental charged-particle multiplicities (open circles) (Refs. 16 and 17) and our predictions (full circles) at the ISR energies (a) 30; (b) 45; (c) 53; (d) 62 GeV.

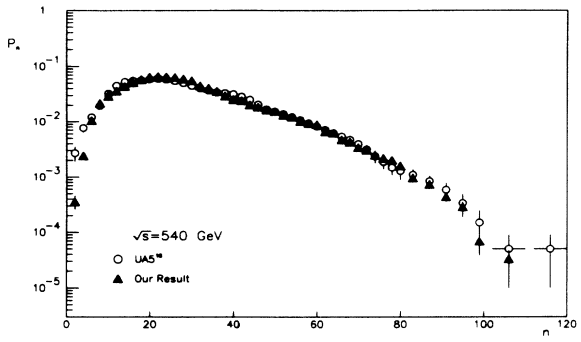

FIG. 14. Our prediction for the charged-particle multiplicity (full circles) and the experimental data (open circles) (Ref. 18) at the Collider energy.

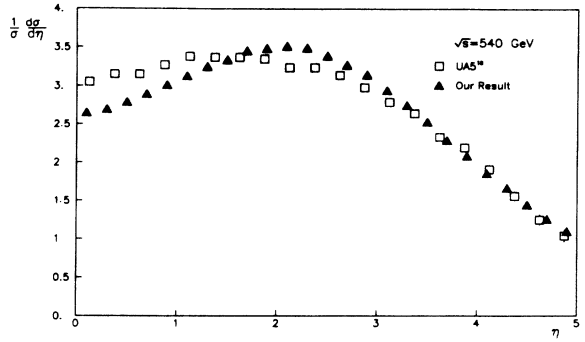

FIG. 16. The experimental pseudorapidity distribution of charged particles (open circles and open boxes) (Ref. 18) compared to our predictions (full triangles) at Collider energy.

to become relevant. We plan to come to this interesting point in the next future.

Getting now to the structure of final states, in Fig. 13 we compare the charged-particle multiplicities in the ISR range with the relevant experimental information.[16,17] Agreement is seen to be quite remarkable. Our prediction for charged-particle multiplicity at Collider energy is compared with the UA5 data[18] in Fig. 14. Note, again, the very good agreement with experiments, particularly in the large multiplicity tail. The quality of the agreement can be further appreciated by looking at Table I, where our predictions for different moments of the multiplicity distributions are compared with the experiments.[16–18]

The comparison of our predictions for the pseudorapidity distributions with ISR[16,17] and Collider data[18] can be seen in Figs. 15 and 16, respectively. Taking into account the discrepancies between the two sets of data at $\sqrt{s}=53$ GeV and our neglect of the particular experimental conditions of the UA5 apparatus, we consider the agreement quite satisfactory.

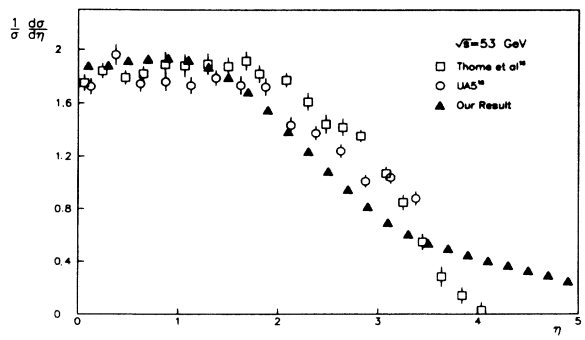

FIG. 15. The experimental pseudorapidity distribution of charged particles (open circles and open boxes) (Refs. 16 and 18) compared to our predictions (full triangles) at the c.m. energy 53 GeV.

VII. COMPARISON WITH OTHER THEORIES

Before concluding it is, perhaps, appropriate to discuss briefly the relationship of this work with other, related, approaches.

The model that is the most akin to the one presented here, and the most thoroughly developed is certainly the dual parton model[19] of Capella, Tran Thanh Van, and collaborators, where the cut Pomeron chains are strictly related to our fire-string decay. However, we should like to stress that the fire-string notion gives a solid theoretical basis to the more phenomenological concept of cut Pomeron chains. So in this respect our approach supports the description of the dual parton model.

As for the particle content of the cut Pomeron chains—in our language, the fire-string decay product—in the dual parton model the very rudimentary model of Feynman and Field is employed with the attendant rather complex parametrizations, which theoretically do not stand on a par with the sophisticated analysis of the fire-string model. On the other hand, the phenomenological Regge aspects of our work is totally similar to the dual parton model.

Finally our fire-string decay has many aspects in common with the Lund model.[20] However we would like to remind the reader that a search of the literature shows that the basic ideas of the fire-string decay were laid down prior to the development of the Lund model.

VIII. CONCLUSIONS

As the discussion of the preceding section shows we may now state with confidence that a good understanding of some important features of the structure of pp ($\bar{p}p$) scattering at high energy can be achieved within the QGD/ACD theoretical framework.

Contrary to the common lore, we have shown that long-distance physics can be conquered in terms of rather simple ideas, which find their theoretical and computational realization in a limited number of parameters. And it is conceivable that, following up the strategy outlined in Ref. 1, we shall be able in the near future to com-

TABLE I. The experimental moments of the multiplicity distributions (a) at the ISR (Refs. 16 and 17) energies for inelastic events and (b) at the Collider (Ref. 18) energy for non-single-diffractive events compared with our calculations. The moments are defined by $D_p=\langle(n-\langle n\rangle)^p\rangle^{1/p}$, $C_p=\langle n^p\rangle/\langle n\rangle^p$.

(a)

	30 GeV			45 GeV		
	Our Res.	Ref. 16	Ref. 17	Our Res.	Ref. 16	Ref. 17
$\langle n\rangle$	9.24	9.54±0.12	9.43±0.18	10.95	11.01±0.17	10.86±0.16
D_2	4.78		5.05±0.11	5.91		5.76±0.10
D_3	5.62		4.32±0.17	6.57		5.20±0.19
$\langle n\rangle/D_2$	1.93		1.87±0.07	1.85		1.89±0.06
C_2	1.27	1.26±0.01	1.29±0.02	1.29	1.29±0.02	1.28±0.01
C_3	2.03	1.86±0.04	1.97±0.06	2.08	1.99±0.05	1.96±0.05
C_4	6.43	3.12±0.11	3.44±0.17	5.23	3.53±0.16	3.41±0.15
	53 GeV			62 GeV		
	Our Res.	Ref. 16	Ref. 17	Our Res.	Ref. 16	Ref. 17
$\langle n\rangle$	11.61	11.77±0.10	11.55±0.17	12.25	12.70±0.12	12.25±0.21
D_2	6.40		6.23±0.10	6.91		6.62±0.10
D_3	6.88		5.55±0.20	7.36		5.65±0.18
$\langle n\rangle/D_2$	1.81		1.85±0.06	1.77		1.85±0.06
C_2	1.30	1.29±0.01	1.29±0.01	1.32	1.30±0.01	1.29±0.01
C_3	2.12	2.01±0.03	1.98±0.05	2.17	2.02±0.03	1.97±0.05
C_4	5.04	3.58±0.09	3.48±0.15	4.99	3.60±0.10	3.40±0.15

(b)

	540 GeV	
	Our Res.	Ref. 18
$\langle n\rangle$	29.46	29.4±1.2
D_2	15.03	15.7±0.5
D_3	15.43	15.7±0.7
D_4	21.73	21.2±0.7
$\langle n\rangle/D_2$	1.96	1.87±0.1
C_2	1.26	1.29±0.03
C_3	1.92	2.01±0.12
C_4	3.43	3.66±0.40

pute these parameters from QCD. Indeed, we should now recall that it is an unchallenged theoretical proposition that the generally accepted picture of QCD, with its perturbative structure at short light-cone distances, is an essentially unstable realization of the underlying gauge-theory Lagrangian, and the ACD Lagrangian just that describes the effective dynamical degrees of freedom around what is most likely the QCD ground state, the chromomagnetic liquid.[1]

Viewed in this light, the good successes in the first steps of the QGD/ACD analysis of the structure of high-energy pp ($\bar{p}p$) scattering provides further support of the growing theoretical evidence in favor of ACD being the correct dynamical realization of the QCD theory. Furthermore, the feasibility of the theoretical analysis of very complicated physical situations, that we have demonstrated in this paper, opens the exciting possibility to investigate many important aspects of low-p_T (long-distance) physics at high energy, that up to now have been either ignored or analyzed with inadequate theoretical models. Freed from the superstition of the hopeless complication, thus calculability of the low-p_T physics, we hope that new interest will arise in these fascinating phenomena, especially in the wake of the large quantity of data that are being produced at the Fermilab Tevatron Collider.

APPENDIX A

The baryon fragmentation function $A_B(p,p',k)$, representing the process of Fig. 1 and described by the diagram in Fig. 17, has been calculated numerically following the QGD/ACD prescriptions[8] by integrating the overlap integral of the QGD baryon wave functions.[10]

In the momentum representation the relevant integral is

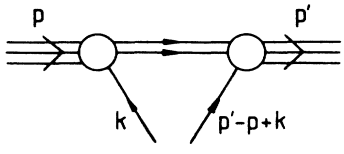

FIG. 17. The diagram representing the dissociation amplitude.

$$A_B(p,p',k)=\int \frac{d^4k_2}{(2\pi)^4}\int \frac{d^4k_3}{(2\pi)^4}\delta_{R^2}(k_2^2-m_2^2)\delta_{R^2}(k_3^2-m_3^2)\chi^{\dagger}_{h'A'}(p';p-p'-k,k_2,k_3)\chi^{hA}(p;k,k_2,k_3)\ , \tag{A1}$$

where $\chi^{hA}(p;k_1,k_2,k_3)$ is the wave function for a baryon of momentum p containing three quarks of momenta k_1,k_2,k_3, whose expression is given in Ref. 10; h,h' are the baryon helicities and $A=(a,\alpha)$, $A'=(a',\alpha')$ are the flavor indices (a,a') and the color indices (α,α'). Notice that the "fat-delta" functions δ_{R^2} in Eq. (A1), defined by

$$\delta_{R^2}(z)=\frac{1}{\pi}\frac{\sin(R^2z)}{z}$$

represent the quark propagators, as discussed in Ref. 11, and make the integral receives the main contribution from the kinematical region, where the quarks are as close as possible to their mass shell.

The features of amplitude of Eq. (A1), when inserted in Eq. (2.4), have been illustrated in Sec. II.

APPENDIX B

Noting that at high energy the longitudinal dynamics is decoupled from the transverse dynamics, we can represent (see Fig. 18) the first-order cross sections $\sigma_i(s)$, for i=2FS,SD,DD, as

$$\sigma_i(s)=\int_0^s ds'\int d^2k_1 d^2k_2 K_i(s,s';\mathbf{k}_1^2,\mathbf{k}_2^2)\ , \tag{B1}$$

where the kernel K_i can be parametrized in the form

$$K_i(s,s';\mathbf{k}_1^2,\mathbf{k}_2^2)=K_i(s,s')\left[\frac{B_1B_2}{\pi^2}\right]e^{-B_1\mathbf{k}_1^2}e^{-B_2\mathbf{k}_2^2} \tag{B2}$$

with

$$\int ds' K_i(s,s')=\sigma_i(s)\ . \tag{B3}$$

Looking at the elastic-scattering amplitude as a "shadow" of the inelastic processes, now, the contribution of the first-order mechanism i, $T_i(s,t)$, to the elastic amplitude

$$A_{\rm el}^{(1)}=is\sum_{i=1}^{3}T_i(s,t)\ . \tag{B4}$$

1. 2FS mechanism

From the diagram in Fig. 19 we can write, at small $t=-\Delta^2$,

$$T_{2FS}(s,t)=\int_0^s ds' K_{2FS}(s,s')\int d^2k_1 d^2k_2 \frac{B_1B_2}{\pi^2}\exp\left[-\frac{B_1}{2}[\mathbf{k}_1^2+(\mathbf{k}_1-\boldsymbol{\Delta})^2]-\frac{B_2}{2}[\mathbf{k}_2^2+(\mathbf{k}_2+\boldsymbol{\Delta})^2]\right]\exp(B_{FS}t)$$
$$=\sigma_{2FS}(s)\exp\left[-\left[\frac{B_1}{4}+\frac{B_2}{4}+B_{FS}\right]\Delta^2\right]\ . \tag{B5}$$

Note that the slope B_{FS}, which does not appear in Eq. (B2), describes here the transverse momentum transferred by the FS's.

For the case in which two vertices are symmetric, $B_1=B_2=B$ leads to

$$b_{2FS}=\frac{B}{2}+B_{FS} \tag{B6}$$

which is the free parameter of the present analysis as discussed in Sec. V.

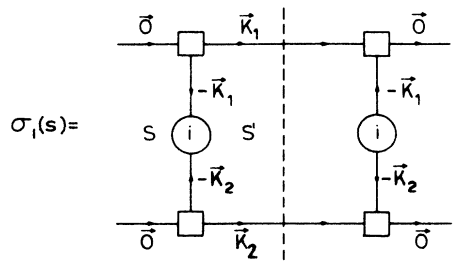

FIG. 18. The diagram showing the contribution to the inelastic cross section, arising from the basic mechanism i=2FS, SD, DD, in the transverse variables $\mathbf{k}_1,\mathbf{k}_2$.

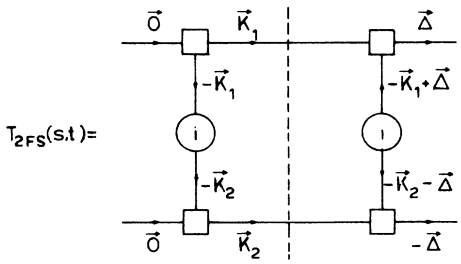

FIG. 19. The diagram showing the contribution to the elastic cross section coming from the "shadow" of the basic inelastic mechanism 2FS.

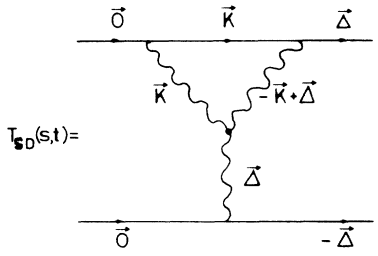

FIG. 20. The diagram showing the contribution to the elastic cross section coming from the "shadow" of the basic single-diffractive mechanism SD.

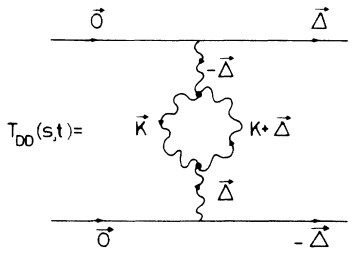

FIG. 21. The diagram showing the contribution to the elastic cross section coming from the "shadow" of the basic double-diffractive mechanism SD.

2. SD mechanism

At high energy we consider the dominant term in Eq. (3.2), namely, the *PPP* contribution, with the following parametrization of the residue functions at small t:

$$\beta_P(t)=\beta_P(0)e^{b_0 t}\ , \tag{B7a}$$

$$g_{3P}(t_1,t_2,t_3)=g_{3P}(0)e^{b_1(t_1+t_2)+b_3 t_3}\ , \tag{B7b}$$

where t_3 refers to the P leg which appears asymmetrically ($t_3=0$) in the single-diffractive cross section. The relevant diagram, shown in Fig. 20, gives the following SD contribution to the elastic amplitude:

$$\begin{aligned}T_{SD}(s,t)&=\sigma_{SD}(s)\int\frac{d^2k}{(2\pi)^2}\exp\{-(b_0+\alpha')[\mathbf{k}^2+(\mathbf{k}-\boldsymbol{\Delta})^2]\}\exp\{-(b_1+\alpha')[\mathbf{k}^2+(\mathbf{k}-\boldsymbol{\Delta})^2]\}\\&\quad\times\exp[-(b_3+b_0+\alpha')\boldsymbol{\Delta}^2]\\&=\sigma_{SD}(s)\exp\{-[\tfrac{1}{2}(b_0+b_1+\alpha')+(b_0+b_3+\alpha')]\boldsymbol{\Delta}^2\}\end{aligned} \tag{B8}$$

with

$$\alpha'=\alpha'_P(0)\ln(s/s_0)\ , \tag{B9}$$

where s_0 is a scale energy. Thus, the contribution of the SD mechanism to the slope of the elastic amplitude is

$$b_{SD}=\tfrac{1}{2}(b_0+b_1+\alpha')+b_0+b_3+\alpha'\ . \tag{B10}$$

3. DD mechanism

Following the same procedure as in the preceding paragraph, now we evaluate the DD contribution to the elastic scattering amplitude, shown in Fig. 21:

$$\begin{aligned}&T_{DD}(s,t)\\&\quad=\sigma_{DD}(s)\exp\{-[2(b_0+\alpha')+2b_3]\boldsymbol{\Delta}^2\}\\&\quad\times\int\frac{d^2k}{(2\pi)^2}\exp\{-2(b_1+\alpha')[\mathbf{k}^2+(\mathbf{k}+\boldsymbol{\Delta})^2]\}\end{aligned} \tag{B11}$$

with the slope

$$b_{DD}=2(b_0+b_3+\alpha')+b_1+\alpha'\ . \tag{B12}$$

Combing back to Eq. (B4), we have calculated the contribution of the three basic mechanisms (2FS, SD, DD) to the elastic-scattering amplitude. In this approximation, the elastic slope is given by

$$\begin{aligned}B_{el}(s)&=2\frac{d}{dt}\ln[\mathrm{Im}\,A_{el}(s,t)]_{t=0}\\&=2\left[b_{2FS}\frac{\sigma_{2FS}}{\sigma^{(1)}}+b_{SD}\frac{\sigma_{SD}}{\sigma^{(1)}}+b_{DD}\frac{\sigma_{DD}}{\sigma^{(1)}}\right].\end{aligned} \tag{B13}$$

[1]The equivalence of the QGD/ACD approach with the QCD Lagrangian realized on a highly nontrivial stable ground state, the chromomagnetic liquid, has now been established. See G. Preparata, Milano Report No. MITH89/1, 1989 (unpublished).

[2]L. Angelini, L. Nitti, M. Pellicoro, G. Preparata, and G. Valenti, Riv. Nuovo Cimento **6**, 1 (1983).

[3]A. Giannelli, L. Nitti, G. Preparata, and P. Sforza, Phys. Lett. **150B**, 214 (1985); E. Ferrari, G. Violini, G. Preparata, L. Angelini, L. Nitti, and M. Pellicoro, Z. Phys. C **41**, 39 (1988).

[4]L. Angelini, L. Nitti, M. Pellicoro, G. Preparata, and G. Valenti, Phys. Lett. **107B**, 446 (1981).

[5]L. Angelini, L. Nitti, M. Pellicoro, G. Preparata, and G. Valenti, Nucl. Phys. **B216**, 83 (1983).

[6]L. Angelini, L. Nitti, M. Pellicoro, and G. Preparata, Phys. Lett. **141B**, 255 (1984).

[7]L. Angelini, L. Nitti, M. Pellicoro, and G. Preparata, Phys. Lett. B **211**, 472 (1988).

[8]For a broad review of QGD, see G. Preparata, in *The Why's of Subnuclear Physics,* edited by A. Zichichi (Plenum, New York, 1979), p. 727.

[9]For a review of ACD, see G. Preparata, in *Fundamental Interactions: Cargèse 1981,* proceedings of the 1981 Cargèse Summer Institute, Cargèse, France, 1981, edited by J. L. Basdevant, D. Speiser, J. Weyers, M. Jacobi, R. Gastmans, and M. Levy (Nato Advanced Study Institute, Series B: Physics, Vol. 85) (Plenum, New York, 1982).

[10]G. Preparata and K. Szego, Phys. Lett. **68B**, 239 (1977); Nuovo Cimento **47A**, 303 (1978).

[11]G. Preparata, Nucl. Phys. **B122**, 29 (1977).

[12]In the early version of QGD/ACD, the massive-quark-model, this Regge-type exchange was called the "primeval Pomeron." See G. Preparata, in *On the Lepton and Hadron Structure,* edited by A. Zichichi (Academic, New York, 1975), p. 54.

[13]A. B. Kaidalov, Phys. Rep. **50**, 157 (1979); G. Alberi and G. Goggi, *ibid.* **74**, 1 (1981).

[14]J. W. Chapman *et al.*, Phys. Rev. Lett. **32**, 257 (1974); M. G. Albrow *et al.*, Nucl. Phys. **B108**, 1 (1976); P. Capiluppi *et al.*, *ibid.* **B70**, 1 (1974); **B79**, 189 (1974); A. E. Brenner *et al.*, Phys. Rev. D **26**, 1497 (1982).

[15](a) U. Amaldi and K. R. Schubert, Nucl. Phys. **B166**, 301 (1980); (b) N. Amos *et al.*, Phys. Lett. **120B**, 460 (1983); **128B**, 343 (1983); (c) UA4 Collaboration, M. Bozzo *et al.*, *ibid.* **115B**, 495 (1982); (d) UA5 Collaboration, G. J. Alner, Z. Phys. C **33**, 1 (1986).

[16]W. Thomè *et al.*, Nucl. Phys. **B129**, 365 (1977).

[17]ABCDHW Collaboration, A. Breakstone *et al.*, Phys. Rev. D **30**, 528 (1984).

[18]UA5 Collaboration, G. J. Alner *et al.*, Phys. Rep. **154**, 247 (1987).

[19]For a review of the dual parton model see, for example, A. Capella, in *Multiparticle Production,* proceedings of the Shandong Workshop, Jinan, Shandong, China, 1987, edited by R. C. Hwa and Xie Qu-bing (World Scientific, Singapore, 1988).

[20]B. Andersson, G. Gustafson, G. Ingelman, and T. Sjostrand, Phys. Rep. **97**, 33 (1983).